materials

MDPI

Article

Acousto-optic cells with phased-array transducers and their application in systems of optical information processing

Vladimir Balakshy [1,2]*, Maxim Kupreychik [1], Sergey Mantsevich [1], and Vladimir Molchanov [3]

[1] Faculty of Physics, Lomonosov Moscow State University; info@physics. msu.ru
[2] Scientific and Technological Centre of Unique Instrumentation of the Russian Academy of Sciences; np@ntcup.ru
[3] Acousto-Optical Research Center, National University of Science and Technology MISIS; press@edu.misis.ru
* Correspondence: balakshy@phys.msu.ru; Tel.: +7-906-075-0295

Received: date; Accepted: date; Published: date

Abstract: The paper presents results of theoretical and experimental studies of anisotropic acousto-optic interaction in a spatially periodical acoustic field created by a phased-array transducer with antiphase excitation of adjacent sections. In this case, contrary to the non-sectioned transducer, light diffraction is absent when the optical beam falls on the phased-array cell at the Bragg angle. However, the diffraction takes place at some other angles (called "optimal") which are situated on the opposite sides in regard to the Bragg angle. The calculations have shown that the diffraction efficiency can reach 100% at these optimal angles in spite of a noticeable acousto-optic phase mismatch. This type of acousto-optic interaction possesses a number of interesting regularities which can be useful at designing acousto-optic devices, such as modulators, deflectors and filters. In the experiment, a paratellurite cell was used with a shear acoustic mode propagating at the angle 9^0 to the crystal plane (001). The transducer had up to 9 antiphase sections. The efficiency of electric–to–acoustic power conversion was 99% at the maximum frequency response, and the ultrasound excitation band extended from 70 to 160 MHz.

Keywords: acousto-optics; phased-array piezoelectric transducers; acousto-optic materials; anisotropic Bragg diffraction; acousto-optic devices.

1. Introduction

The basis of modern acousto-optic (AO) devices, applied in systems of optical information processing, are AO cells usually made of crystals of a certain cut. Ultrasonic waves are excited by piezoelectric plates attached to one of the cell faces. In these instruments, a type of light diffraction by ultrasound close to the Bragg regime is usually used [1-3]. The regime is realized at sufficiently high acoustic frequencies (usually over 100 MHz) and allows us to create devices with good performance and low light losses. However, as a disadvantage, one can note high selectivity of this type of interaction, which means a strong dependence of AO effect magnitude on the frequency of ultrasound f, the angle of light incidence θ_0 and the wavelength of optical radiation λ. An important characteristic of the effect is the Bragg angle θ_B. When the light beam falls at a Bragg angle (phase-matching condition), the most effective light scattering into the diffraction order occurs, and the decrease in the diffraction efficiency by 3 dB determines the boundary of the AO interaction region.

In principle, the interaction region can be extended by reducing the length of AO interaction L (the width of the acoustic beam in the direction of light propagation), but this will result in reducing

the diffraction efficiency and/or increasing the acoustic power required for obtaining a necessary diffraction efficiency. Taking into consideration this negative situation, A. Korpel et al. [4] proposed to use a step-sectional piezoelectric transducer for excitation of an acoustic beam with a rotating radiation pattern. In their AO cell, the acoustic wave front rotated with ultrasound frequency, adjusting to the optimal angle of light incidence.

However, such a cell was very difficult in manufacturing, so planar structures shown in Figure 1 were then proposed [5-8]. In the first variant (Figure 1a), one piezoelectric plate is used, and separate sections are formed by partitioning the internal and external electrodes. In another case (Figure 1b), the internal electrode is first made solid, and then grooves are sawn at the final stage. The pictures show the AO cells with transducers containing four sections that are connected electrically in series, but in such a way that the direction of the electric field (shown by the arrows) in the adjacent sections is opposite. Due to this, acoustic beams from each section are excited with phase shift of π, and a system of equivalent wave fronts (shown by two dashed lines) is formed, turned by an angle Ψ relative to the transducer plane. This angle is determined by the expression

$$\Psi = \pm\frac{\Lambda}{2d} = \pm\frac{V}{2fd}, \quad (1)$$

where $\Lambda = V/f$ is the acoustic wave length, V is its velocity and d is the period of the transducer array.

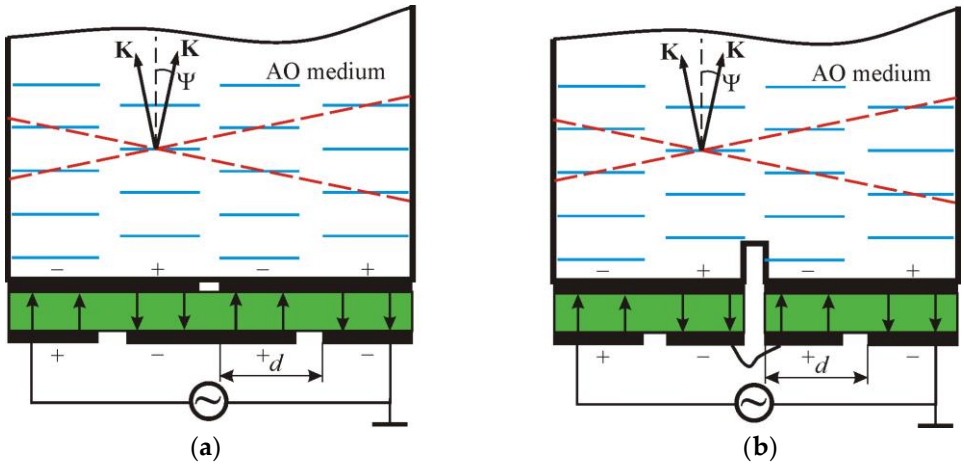

Figure 1. Two variants of flat phased-array transducers with antiphase excitation of adjacent sections.

In comparison with a homogeneous (non-sectioned) transducer, here the transfer function of the AO cell contains two main maxima, which are located symmetrically with respect to the Bragg angle θ_B, as shown in Figure 2 with curve *1*. It follows from the figure that AO diffraction is absent when the light beam falls at the Bragg angle ($\theta_0 = \theta_B$). This is due to the fact that partial diffracted waves generated in neighboring acoustic beams are phase-shifted by π and therefore damp each other during interference. However, there are other maxima situated equidistantly with the period Λ/d, which are inscribed into dashed curve *2* showing the radiation pattern of a separate section of the transducer. The width of the maxima is equal to Λ/md, where m is the number of periods of the transducer array. Thus, we can conclude that in the case of the phased-array transducer, the concept of the Bragg angle as the angle of light incidence, at which the phase matching condition is fulfilled and the maximum diffraction efficiency is observed, is incorrect. Here we can talk about the optimal angles of light incidence $\theta_{opt} = \theta_B \pm \Lambda/2d = \theta_B \pm V/2fd$, which correspond to the maximal scattering of light, although the phase matching condition is violated. It can be noticed that these optimal angles conform to the conventional Bragg angles, when light falls on the equivalent wave fronts. Consequently, such a structure of the acoustic field can be considered as a superposition of two fields excited by two solid piezoelectric transducers rotated relative to each other by the angle Λ/d.

Our calculations have shown that the diffraction efficiency can reach here 100%, despite a noticeable phase mismatch. But this requires a slightly higher acoustic power [9,10].

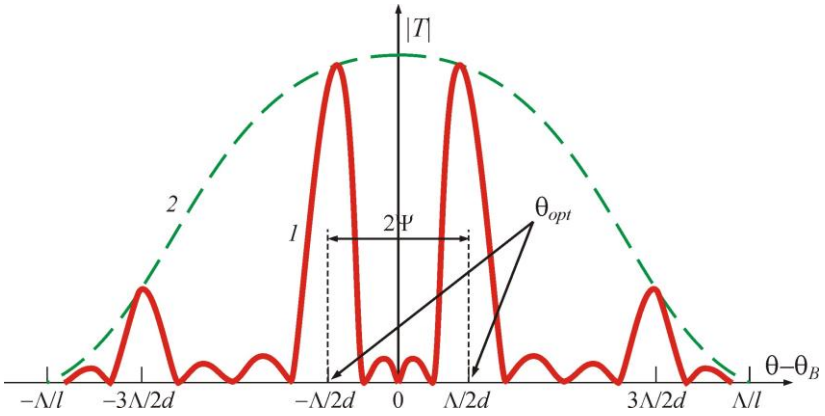

Figure 2. Radiation patterns of four-sectioned (*1*) and one-sectioned (*2*) transducers.

As follows from (1), when the ultrasound frequency decreases, the main lobes of the transducer radiation pattern diverge. Therefore, if one chooses the true angle of light incidence, the equivalent wave front will rotate, adjusting to the changing Bragg angle. This adjustment will not be complete, since the Bragg angle depends on the frequency linearly, but the angle of rotation Ψ – in accordance with the hyperbolic law. The best correction of the Bragg angle is obtained when $d\theta_{opt}/df = 0$. This condition is satisfied at the frequency

$$f^* = V\sqrt{\frac{n}{\lambda d}}, \tag{2}$$

where n is the refractive index of the AO medium and λ is the optical wave length in vacuum. Thus, by selecting an appropriate period d of the phased-array transducer, we can set the operating point f^* in any desired frequency range.

The interest to the phased-array transducers weakened noticeably after the anisotropic AO diffraction entered the practice of acousto-optics [11]. The main advantage of anisotropic diffraction consists in a significantly more complicated frequency dependence of the Bragg angles in comparison with the AO interaction in an isotropic medium. This feature makes it possible to choose optimal interaction geometry for each separate AO device. For example, for AO deflectors the optimal area is that where $d\theta_B/df \to 0$, whereas for AO video-filters is the area with $d\theta_B/df \to \infty$ [1,2].

The use of the phased-array transducers in combination with anisotropic diffraction gives more complicated types of Bragg curves, which open up new opportunities for improvement of AO device characteristics [12,13]. Therefore, the aim of this work is studying peculiarities of anisotropic AO interaction in the acoustic field created by the phased-array transducers with antiphase excitation of adjacent sections.

2. Acousto-optic effect in the field of phased-array transducer

Figure 3 illustrates the statement of the problem. It is considered the most general case of an anisotropic medium in which acoustic beams propagate with a walk-off angle α. We assume that the inclined phase grating created by the acoustic wave occupies the area of space between the infinite planes $x = 0$ and $x = L$. The wave vector of ultrasound is inclined at an angle α. The width of each acoustic column is l. Therefore, the second column occupies the space between the planes $x = l + a$ and $x = 2l + a$, where a is the gap between the acoustic beams, etc. Thus, the period of the transducer structure is $d = l + a = l(1 + \xi)$. The initial acoustic phase in the first column is equal to $\Phi = 0$, in the following column is $\Phi = \pi$; at that the phase shift between adjacent beams is equal to $\Delta\Phi = \pi$. The total number of beams is m.

Consider for this structure the regime of anisotropic diffraction with Bragg scattering of light into two diffraction orders: zero and +1st or zero and –1st. In this case, the calculation has to take into account two optical plane waves. The first wave is falling; it is characterized by the wave vector $\mathbf{k_0}$ and the incidence angle θ_0. The second one is a diffracted wave with the wave vector $\mathbf{k}_{\pm1}$ and the diffraction angle $\theta_{\pm1}$. The interaction of these waves is described by the following system of equations [14,15]:

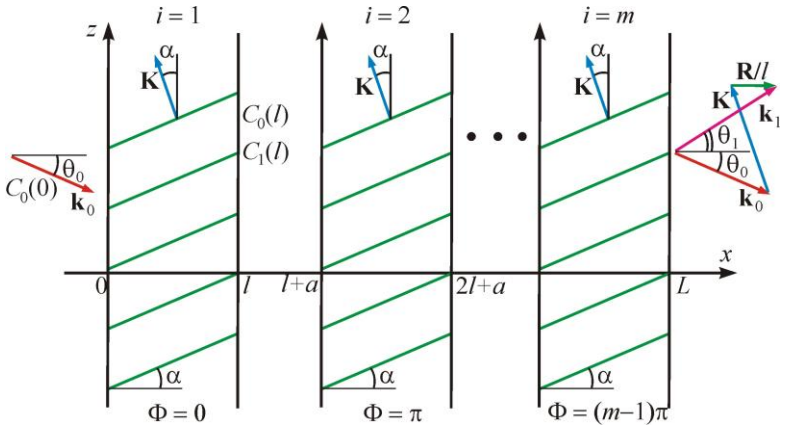

Figure 3. Statement of the problem of AO interaction in the field of phased-array transducer.

$$\begin{cases} \dfrac{dC_0}{dX} = \pm\dfrac{\Gamma}{2} C_{\pm1} \exp\left[\pm j\left(R_{\pm}X - \Phi\right)\right] \\ \dfrac{dC_{\pm1}}{dX} = \mp\dfrac{\Gamma}{2} C_0 \exp\left[\mp j\left(R_{\pm}X - \Phi\right)\right] \end{cases} \tag{3}$$

where, for the convenience of numerical calculations, dimensionless values are introduced: the normalized amplitudes of the incident C_0 and diffracted $C_{\pm1}$ waves, the coordinate $X = x/l$, the Raman–Nath parameter

$$\Gamma = \frac{2\pi l \Delta n}{\lambda \cos\theta_0} \tag{4}$$

and dimensionless phase mismatch

$$R_{\pm} = \frac{2\pi}{\lambda} l \left[n_0 \cos\theta_0 \mp \frac{\lambda f}{V} \sin\alpha - \sqrt{n_{\pm1}^2 - \left(n_0 \sin\theta_0 \pm \frac{\lambda f}{V} \cos\alpha \right)^2} \right] \tag{5}$$

In these formulas, n_0 and $n_{\pm1}$ are the refractive indices for incident and diffracted light, Δn is the amplitude of the refractive index change under the action of the acoustic wave. A wave vector diagram of AO interaction is shown in Figure 3 on the right; it corresponds to the vector relationship [1]:

$$\mathbf{k}_0 + \mathbf{K} + \frac{\mathbf{R}_{\pm}}{l} = \mathbf{k}_{\pm1} \tag{6}$$

Here we have taken into consideration that the phase mismatch vector $\mathbf{R}_{\pm}$ is perpendicular to the boundaries of the acoustic beams.

When the light waves propagate in the periodic acoustic field, the optical energy is redistributed between them. Our task is to find the amplitudes of the waves at the output of the structure: $C_0(L)$ and $C_1(L)$. This can be fulfilled by recording a recurrence relation connecting the input and output fields for the *i*-th acoustic beam. The boundary conditions at the input have the following form:

$$\begin{cases} E_0(x) = E_i C_0^{(i)} \exp\left[\mathrm{j}(\omega_o t - k_0 \cos\theta_0 x - k_0 \sin\theta_0 z)\right] \\ E_{\pm1}(x) = E_i C_{\pm1}^{(i)} \exp\left[\mathrm{j}(\omega_{\pm1} t - k_{\pm1} \cos\theta_{\pm1} x - k_{\pm1} \sin\theta_{\pm1} z)\right] \end{cases}, \quad (7)$$

where E_i is the amplitude of the incident optical wave, ω_0 and $\omega_{\pm1}$ are the frequencies of incident and diffracted light; at that $\omega_{\pm1} = \omega_0 \pm \Omega$, and $\Omega = 2\pi f$ is the cyclic frequency of ultrasound. Solving Equations (3) with boundary conditions (7), we obtain the expressions for the amplitudes at the input of the (i + 1)-st acoustic column:

$$C_0^{(i+1)} = \left[C_0^{(i)} \left(\cos\frac{\sqrt{\Gamma^2 + R_\pm^2}}{2} \mp \mathrm{j}\frac{R_\pm}{2} \operatorname{sinc}\frac{\sqrt{\Gamma^2 + R_\pm^2}}{2\pi} \right) \pm C_{\pm1}^{(i)} \frac{\Gamma}{2} \operatorname{sinc}\frac{\sqrt{\Gamma^2 + R_\pm^2}}{2\pi} \exp(\mp \mathrm{j}\Phi) \right] \exp\left(\pm \mathrm{j}\frac{R_\pm}{2} \right) \quad (8)$$

$$C_{\pm1}^{(i+1)} = \exp\left(\mp \mathrm{j}\frac{R_\pm}{2} \right) \left[C_{\pm1}^{(i)} \left(\cos\frac{\sqrt{\Gamma^2 + R_\pm^2}}{2} \pm \mathrm{j}\frac{R_\pm}{2} \operatorname{sinc}\frac{\sqrt{\Gamma^2 + R_\pm^2}}{2\pi} \right) \mp C_0^{(i)} \frac{\Gamma}{2} \operatorname{sinc}\frac{\sqrt{\Gamma^2 + R_\pm^2}}{2\pi} \exp(\pm \mathrm{j}\Phi) \right] \exp\left[\pm \mathrm{j}R_\pm (1 + \xi) \right] \quad (9)$$

Here the phase shift, introduced by the area of empty space between the acoustic columns, is taken into account [16]:

$$C_0(l + a) = C_0(l), \qquad C_{\pm1}(l + a) = C_{\pm1}(l) \exp\left[\pm \mathrm{j}R_\pm (1 + \xi) \right]. \quad (10)$$

However, the equal phase shift $\exp\left[-\mathrm{j}k_0 l \cos\theta_0 (1 + \xi) \right]$ is omitted. In Equations (3)-(10) the upper sign corresponds to light scattering into the +1st order, while the lower sign does to the –1st order.

In acousto-optics, the angles of incidence and diffraction are usually calculated from the front of the acoustic wave. In accordance with this, we introduce angles $\varphi_0 = \theta_0 - \alpha$ and $\varphi_{\pm1} = \theta_{\pm1} - \alpha$. The condition of phase matching $R_\pm = 0$ determines the Bragg angle:

$$\sin\varphi_B = \mp \frac{\lambda f}{2 n_0 V} \left[1 + \frac{V^2}{\lambda^2 f^2} \left(n_0^2 - n_{\pm1}^2 \right) \right]. \quad (11)$$

Expression (11) indicates that the acoustic walk-off does not affect the AO phase matching. However, the parameters Γ and $R_\pm$ depend on the walk-off angle α, as well as the optimal angles θ_{opt}. This means a change in the AO interaction range and, consequently, in diffraction characteristics [17].

3. Computation results

This section presents results of our calculations fulfilled for an acoustic field created by a phased-array transducer in a paratellurite (TeO_2) crystal. They take into account the optical activity of the material, since for the considered diffraction variants, the optical beams propagate close to the optical axis of the crystal, and the optical activity can have a noticeable effect on diffraction characteristics. The calculations are performed for the crystallographic plane $(1\bar{1}0)$, when a shear acoustic wave propagates at an angle of $\chi = 4°$ to the plane (001). For this acoustic mode, the velocity is $V = 0.632 \cdot 10^5$ cm/s and the walk-off angle is $\alpha = 35°$.

Figure 4a demonstrates frequency dependences of the Bragg angles for optical wavelength $\lambda = 0.633$ μm. The four curves correspond to different polarizations of incident light (ordinary "*o*" or extraordinary "*e*") and to the scattering of light into the +1st or –1st orders of diffraction. For example, branch *+1e* characterizes the diffraction of the *e*–wave into the +1st order. Points D and T indicate areas optimal for AO deflectors and video-filters, accordingly [1,2].

Figure 4b displays the AO interaction area separatly for branch *+1e* in coordinates $\varphi_0 - f$. The calculations are carried out for the case of homogeneous (non-sectioned) transducer with a width of

l = 1 mm. The diffraction efficiency $\varsigma = |C_{+1}|^2$ is done in the color scheme: from zero (dark blue) to one (dark red). The values $\zeta = 1$ correspond to the Bragg angles. The fine structure in the picture is caused by the lateral maxima of the function $\mathrm{sinc}(\bullet)$ in Equation (9). The horizontal sections of the pattern determine frequency characteristics of AO interaction $\varsigma(f)$ for specified incidence angles of light, and the vertical sections determine angular characteristics $\varsigma(\varphi_0)$. The shape of the area reproduces curve *+1e* in Figure 4a, and its width is defined primarily by the size of the transducer l.

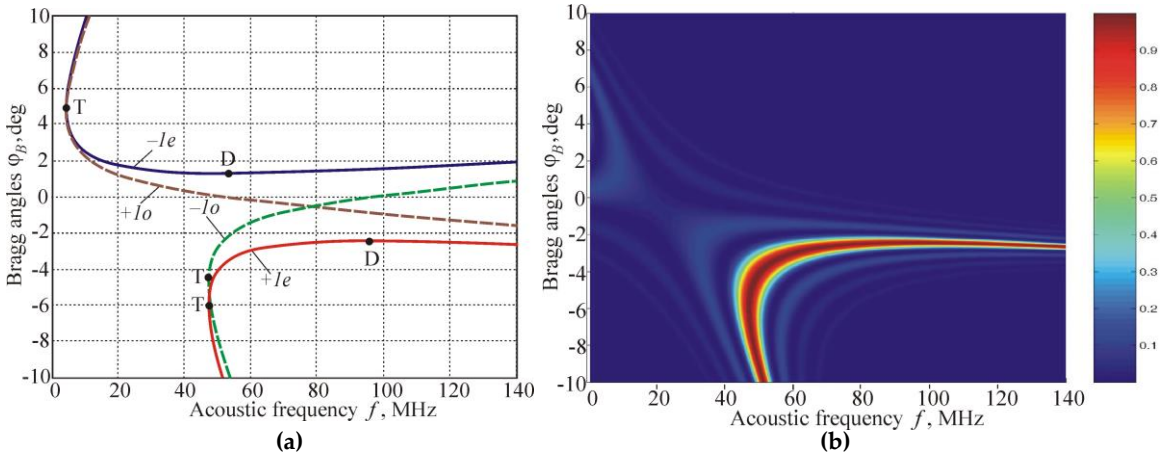

Figure 4. AO interaction in a paratellurite crystal. (**a**) Frequency dependencies of the Bragg angles in the case of light scattering in +1st and –1st diffraction orders at different polarizations of incident optical radiation; (**b**) The area of AO interaction when the optical beam with extraordinary polarization diffracts into +1st order.

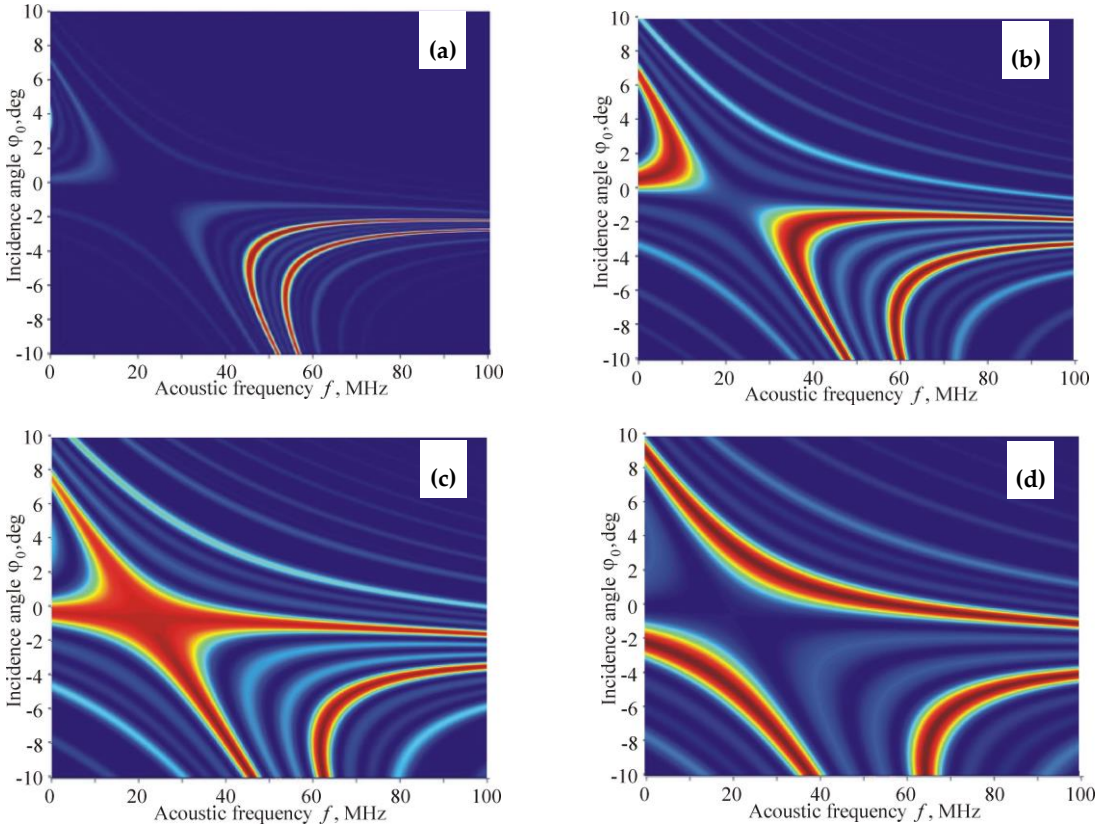

Figure 5. AO interaction areas for branch *+1e* in the case of m = 4 and different width of individual sections: **(a)** l = 0.4 mm; **(b)** l = 0.15 mm; **(c)** l = 0.11 mm; **(d)** l = 0.07 mm.

In the case of a phased-array transducer with antiphase excitation of adjacent sections, the situation changes cardinally. Figure 5 shows this change when the period of structure d decreases. In these calculations, the number of sections is chosen equal to $m = 4$ and the normalized gap between sections is $\xi = 1$.

We see from Figure 5 that for large periods of the transducer structure, a common area of AO interaction splits into two symmetrical domains (Figure 5a). Then an additional domain appears from the side of low ultrasound frequencies (Figure 5b). Thereafter the left domains merge and form a common area with a very complex shape (Figure 5c). Finally, this area splits and three non-overlapping domains form (Figure 6d). It should be noted that such unusual dynamics of AO interaction areas differs significantly from the variant of a homogeneous (non-sectioned) acoustic field. This can be considered as an advantage of the phased-array transducers, because at designing AO devices we can get the optimal geometry of interaction in the most convenient frequency range.

Of particular interest is the case of Figure 5c with a completely unique AO interaction structure characterized by low angular and frequency selectivity. To evaluate this result, one has to take into account that high selectivity of the Bragg diffraction in many AO devices is an interfering factor that leads to a decrease in the frequency and angular ranges of AO interaction and, consequently, to a deterioration of characteristics of AO devices in resolution and operation speed. Figure 5c proves that using the same AO cell, both collimated light beams and image-carrying beams can be processed in a wide frequency range.

Two special points D and T on the Bragg curves are pointed out in Figure 4a. They determine the optimal AO interaction geometry for deflectors and video-filters [1,2]. In the case of anisotropic diffraction in uniaxial crystals, these points never coincide. This means that different AO interaction geometries must be applied at creating deflectors and filters. Our research has shown that this problem can be solved by using phased-array transducers, as Figure 5c demonstrates.

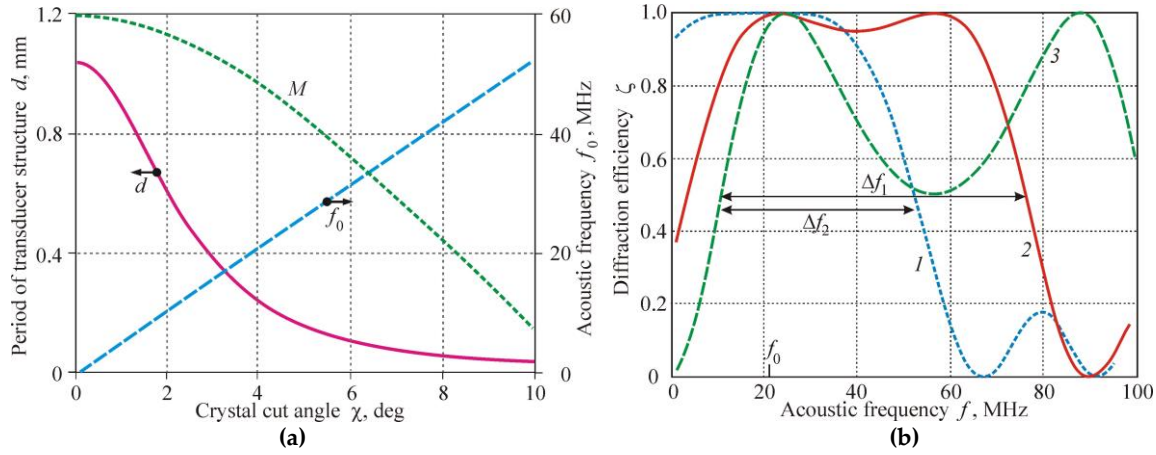

Figure 6. Characteristics of low-selective area shown in Figure 5c. **(a)** Operating frequency f_0, period of transducer structure d and figure of merit M as functions of crystal cut angle χ; **(b)** Frequency characteristics at different incidence angles φ_0.

Figure 6 displays characteristics of this unusual AO geometry. In Figure 6a the operating frequency f_0, which corresponds to the coinciding points D and T, is presented in the dependence of the crystal angle χ and the period of the transducer structure d. The divergence angle between the incident and diffracted beams $\delta\varphi$ (important characteristic for video-filters) increases with the acoustic frequency according to the formula $\delta\varphi \approx \lambda f_0 / nV$. Unfortunately, this positive dependence is accompanied by decreasing the AO figure of merit M (green curve in Figure 6a), which falls from

maximum value $M = 1200 \cdot 10^{-18}$ s³/g at $\chi = 0°$ till $M = 42 \cdot 10^{-18}$ s³/g at $\chi = 10°$ [1,2]. Figure 6b shows detailed characteristics related to the case $f_0 = 21$ MHz ($\chi = 4°$). The frequency dependences are constructed for different angles of light incidence: $\varphi_0 = -0.5°$ (*1*), $\varphi_0 = -1°$ (*2*), and $\varphi_0 = -1.4°$ (*3*). It is seen that the frequency range $\Delta f_1 = 65$ MHz is confirmed to the angular range $\Delta\varphi_0 = 0.4°$, while the range $\Delta f_2 = 42$ MHz can be realized in the angular range $\Delta\varphi_0 = 0.9°$.

The calculation of the AO interaction areas for the variant of ordinary polarization of incident light (branch *+1o* in Figure 4a) gives a significantly different result. The phased-array transducer also leads to splitting the interaction area into two domains. However, the change of these domains with varying the period *d* of transducer structure is greatly different in comparison with the variant discussed above: the region with extremely low angular and frequency selectivity does not appear at all, as seen in Figure 7.

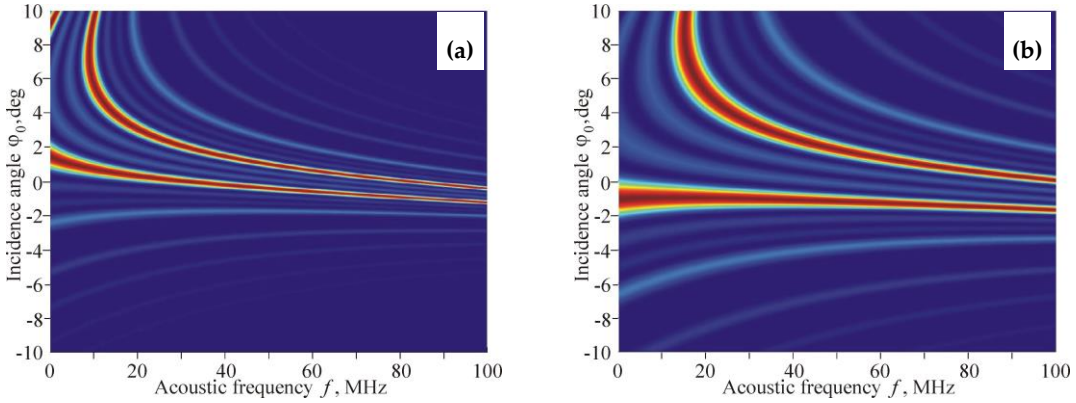

Figure 7. AO interaction areas for branch *+1o* in the case of $m = 4$ and different width of individual sections: **(a)** $l = 0.15$ mm; **(b)** $l = 0.07$ mm.

The comparison of the AO interaction areas for the branches *+1e* and *+1o* allows us to note another interesting and practically important feature, which is fundamentally impossible in the case of AO diffraction in the homogeneous acoustic field. Figure 8 demonstrates frequency dependences of the optimal angles of light incidence φ_{opt} , combined for branches *+1e* and *+1o*. The graphs show

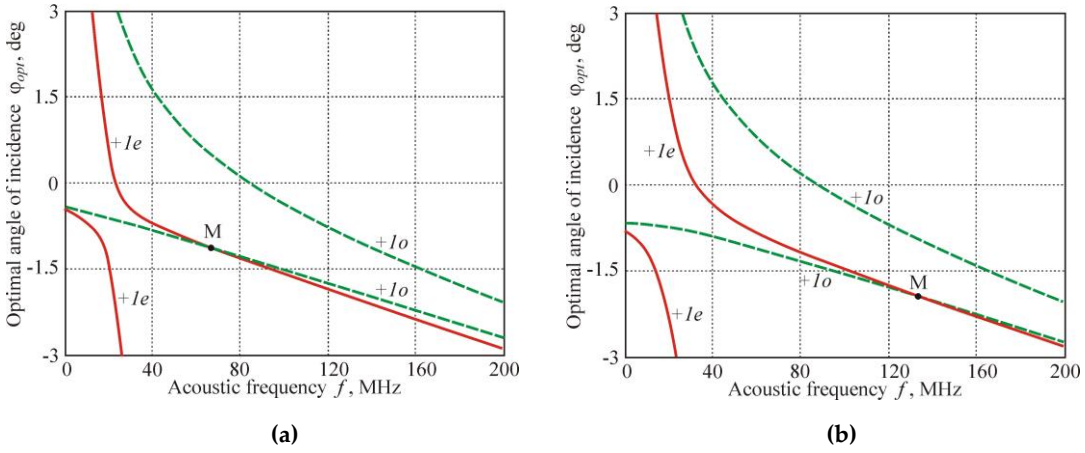

Figure 8. Frequency dependences of optimal angles for branches *+1e* and *+1o*: calculation for **(a)** $d = 0.22$ mm and **(b)** $d = 0.2$ mm.

that the curves, belonging to different diffraction orders *+1e* and *+1o*, intersect at the point M at the frequency f = 67 MHz (Figure 8a) or f = 134 MHz (Figure 8b). This means that at these frequencies the optical waves with ordinary and extraordinary polarizations have to diffract into the same diffraction maximum of the +1st order. Such AO interaction geometry makes it possible to modulate the intensity of unpolarized light beams without optical losses.

In this regard, it should be noted that the problem of AO modulation of unpolarized light has existed since the early 60-ies of the last century and has not yet received an effective solution. The easiest way is to search for cuts of crystals with close values of AO figure of merit M for both optical eigenmodes [1]. A suitable material is a lead molybdate ($PbMoO_4$) [1,18]. However, this crystal is characterized by a relatively small value of AO figure of merit $M = 36 \cdot 10^{-18}$ s³/g and, most importantly, has bad thermophysical properties. Modulators based on the paratellurite crystal with a longitudinal acoustic wave along the Z axis are commercially available, but this cut of the crystal is characterized by a noticeable difference in the figure of merit for the ordinary and extraordinary waves: $M_o = 30 \cdot 10^{-18}$ s³/g and $M_e = 22 \cdot 10^{-18}$ s³/g. In addition, we can also note an exotic scheme of AO modulator with two multidirectional acoustic beams having different frequencies [19].

Contrary to that, we propose a significantly simpler variant of the modulator based on a paratellurite crystal with a phased-array transducer. In this device, the figure of merit coefficients for both optical eigenmodes are the same (due to anisotropic type of diffraction) and equal to $M = 800 \cdot 10^{-18}$ s³/g (for $\chi = 4°$). The position of the operating point M in Figure 8 is determined by the period of the transducer structure d. Choosing the period of the phased array transducer, one can change the operating point in a wide frequency range. Similar variants of the modulator are possible for other cuts of the paratellurite crystal.

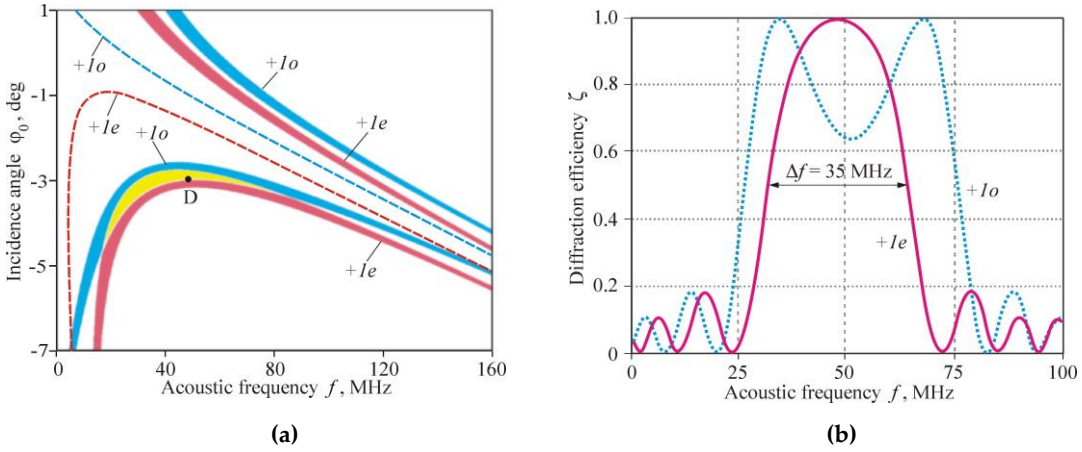

Figure 9. AO deflector of non-polarized light. **(a)** Combined areas of AO interaction for *+1e* (red color) and *+1o* (blue color) diffraction branches; the overlap area is shown by yellow color; **(b)** Frequency characteristics of the AO deflector in the case of unpolarized light.

A similar idea can be implemented for creating AO deflectors intended for scanning of unpolarized optical beams. Figure 9a illustrates this situation for the variant $\lambda = 1.5$ μm, $\chi = 2°$, $m = 8$, and $d = 0.24$ mm. Here the dashed curves demonstrate frequency dependences of the Bragg angles for a non-sectioned transducer, whereas the AO interaction domains for the

phased-array transducer are shown by red and blue colors. The yellow color represents the overlap area. Letter D shows the position of the deflector operating point at $f = 49$ MHz and $\varphi_0 = 3°$.

Frequency characteristics of this deflector for the incidence angle $\varphi_0 = 3°$ is presented in Figure 9b. Two curves relate to different polarizations of incident light. It is seen that the common frequency band is $\Delta f = 35$ MHz. This means that such a deflector can provide optical beam scanning in an angular range of $\Delta\varphi = (\lambda/nV)\Delta f = 2.1°$ with spatial resolution $N = (w/V)\Delta f = 570$ resolvable points when the optical aperture of the AO cell is $w = 1$ cm.

3. Experimental results

Experimental studies were carried out with an AO cell made of a paratellurite crystal. An acoustic wave in the form of a slow shear mode was excited in the crystallographic plane $(1\bar{1}0)$ at an angle $\chi = 9°$ to the direction [110]. For this crystal cut, the sound velocity is equal to $V = 0.69 \cdot 10^5$ cm/s and the walk-off angle is $\alpha = 52.5°$. A phased-array transducer was made of an *X*-cut lithium niobate crystal with an electro-mechanical coupling coefficient $k = 68\%$. The transducer had $m = 9$ sections with a width of $l = 2$ mm each and a relative gap between the sections of $\xi = 0.2$ (Figure 10a). Thus, the total length of the transducer in the direction of light propagation was $L = 2.12$ cm. To effectively excite ultrasound, a RF generator was matched with the transducer with the help of reactive elements – an inductance coil and a capacitor. The efficiency of electric-to-acoustic power conversion in the maximum of the frequency characteristic was 99%, and the ultrasound excitation band extended from 70 to 160 MHz.

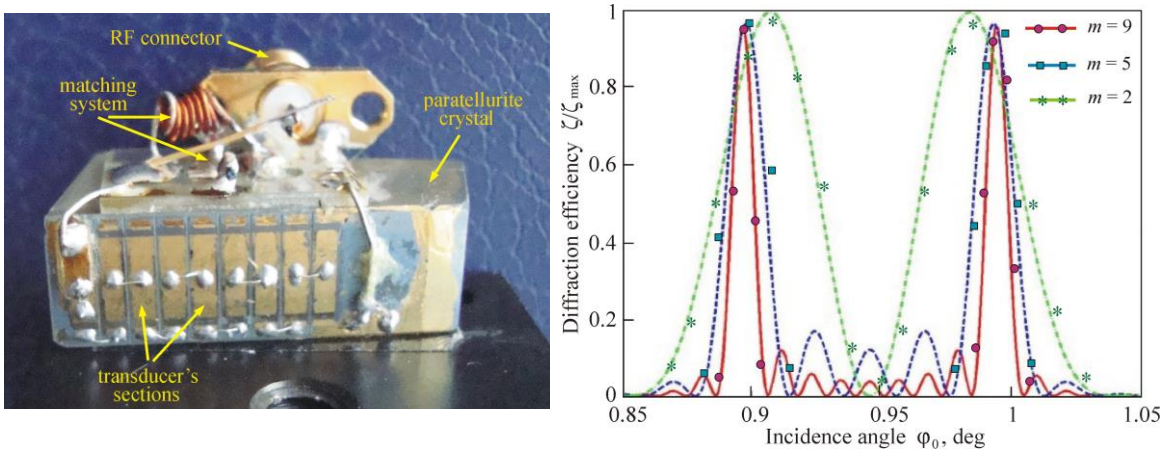

(a) **(b)**

Figure 10. Experimental results. **(a)** AO cell with 9-section transducer; **(b)** Angular characteristics of the AO diffraction for different number of connected sections: $m = 9$ (red), 5 (blue), and 2 (green).

Figure 10 shows angular characteristics of AO interaction (normalized diffraction efficiency ζ/ζ_{max} as a function of the incidence angle φ_0) obtained at the acoustic frequency $f = 105$ MHz. The measurements were fulfilled at scattering of the ordinary polarized optical radiaction with a wavelength of $\lambda = 0.53$ μm into the +1st diffraction order. The red curve relates to the case when all 9 sections were connected in series. In good agreement with calculations, the angular characteristic consists of two main maxima located symmetrically on different sides of the Bragg angle. Decreasing of the number of sections results in broadening the maxima and reducing their intensity. In our experiment, for the convenience of comparing the results, the ultrasound power was adjusted inversely proportional to the number of sections.

4. Conclusions

In this paper, we have presented results of a study of anisotropic Bragg diffraction of light in a spatially periodical acoustic field created by a sectioned piezoelectric transducer with antiphase excitation of adjacent sections. The problem of AO interaction in this periodical acoustic field is solved with taking into account the strong optical and acoustic anisotropy of the interaction medium, typical for many crystals used in modern acousto-optics. Numerical calculations are performed for an AO cell made of paratellurite crystal with the shear acoustic mode propagating at an angle $\chi = 4°$ to the plane (001) of the crystal. It is shown that the AO interaction in such a structure is absent when the optical beam falls at the Bragg angle. However, there exist angles of incidence, called "optimal", at which the diffraction efficiency can reach 100%, despite the violation of the phase matching condition. The areas of interaction for different periods of the transducer structure are calculated. A number of unusual regularities of AO scattering of light is established, which can be useful in the development of AO devices of a new type. In particular, the possibility of implementing a nonpolarized light modulator is shown, which has to have significantly better characteristics than the currently known devices. Preliminary experimental studies were performed with a paratellurite cell, the number of sections of which varied from 9 to 2.

Author Contributions: Conceptualization, Vladimir Balakshy; Investigation, Maxim Kupreychik, Sergey Mantsevich and Vladimir Molchanov; Methodology, Vladimir Molchanov; Resources, Sergey Mantsevich and Vladimir Molchanov; Software, Maxim Kupreychik; Supervision, Vladimir Balakshy; Writing – original draft, Maxim Kupreychik; Writing – review & editing, Vladimir Balakshy.

Funding: This research was funded in part by Russian Science Foundation (RSF), grant number 19-19-00606.

Conflicts of Interest: The authors declare no conflict of interest.

References

1. Balakshy, V.I.; Parygin, V.N.; Chirkov, L.E. *Physical Principles of Acousto-Optics*; Radio & Svyaz: Moscow, Russia, 1985.
2. Das, P.K.; DeCusatis, C.M. *Acousto-Optic Signal Processing: Fundamentals and Applications*; Artech House: New York, USA, 1991.
3. Xu, J.; Stroud, R. *Acousto-Optic Devices*; Wiley: New York, USA, 1992.
4. Korpel, A.; Adler, R.; Desmares, P.; Watson, W. A television display using acoustic deflection and modulation of coherent light. *Proc. IEEE* **1966**, *54(10)*, 1429-1437; **doi:** 10.1109/PROC.1966.5129.
5. Coquin, G.A.; Griffin, J.P.; Anderson, L.K. Wide-band acousto-optic deflectors using acoustic beam steering. *IEEE Trans. Son. Ultrason.* **1970**, *SU-17(1)*, 34-40; **doi:** 10.1109/T-SU.1970.29542.
6. Alphonse, G.A. Broadband acoustooptic deflectors: new results. *Appl. Opt.* **1975**, *14(1)*, 201-207; **doi:** doi.org/10.1364/AO.14.000201.
7. Kim, S.; Gao, L.; Wagner, K.; Weverka, R.; McLeod, R. Acousto-optic tunable filter using phased-array transducer with linearized RF to optical frequency mapping. *Proc. SPIE* **2005**, *5953*, 59530M; **doi:** 10.1117/12.622623.
8. Antonov, S.N.; Vainer, A.V.; Proklov, V.V.; Rezvov, Yu.G. Extension of the angular scanning range of the acousto-optic deflector with a two-element phased-array piezoelectric transducer. *Techn. Phys.* **2013**, *58(9)*, 1346-1351; **doi:** 10.1134/S1063784213090053.
9. Balakshy, V.I.; Linde, B.B.J.; Vostrikova, A.N. Acousto-optic interaction in a non-homogeneous acoustic field excited by a wedge-shaped transducer. *Ultrasonics* **2008**, *48(5)*, 351-356; **doi:** 10.1016/j.ultras.2008.01.001.
10. Mantsevich, S.N.; Balakshy, V.I. Acousto-optic interaction in an inhomogeneous acoustic field. *Opt. & Spectr.* **2015**, *118(4)*, 617-622; **doi:** 10.1134/S0030400X15040153.
11. Dixon, R.W. Acoustic diffraction of light in anisotropic media. *IEEE J. Quant. El.* **1967**, *QE-3(2)*, 85-93; **doi:** 10.1109/JQE.1967.1074447.

12. Voloshin, A.; Balakshy, V.; Mantsevich, S. Unpolarized light diffraction in an acoustic field created by a phased array transducer. Proc. 2016 IEEE Int. Ultrasonics Symp., Tours, France, **2016**, 767-770; **doi:** 10.1109/ULTSYM.2016.7728646.
13. Balakshy, V.I.; Kupreychik, M.I.; Mantsevich S.N. Light diffraction on ultrasound in a spatially periodic acoustic field. *Opt. & Spectr.* **2019**, *127(4)*, 712-718; **doi:** 10.1134/S0030400X19100059.
14. Balakshy, V.I.; Voloshin, A.S. Acousto-optic interaction in crystals with large acoustic anisotropy. *Opt. & Spectr.* **2011**, *110(5)*, 788-794 ; **doi:** 10.1134/S0030400X11050031.
15. Balakshy, V.I.; Voloshin, A.S.; Molchanov, V.Ya. Anisotropic light diffraction in crystals with a large acoustic-energy walk-off. *Opt. & Spectr*. **2014**, *117(5)*, 801-806; **doi:** 10.1134/S0030400X14110046
16. Pozhar, V.E.; Pustovoit, V.I. Consecutive collinear diffraction of light in several acoustooptic cells. *Sov. J. Quant. Electron*. **1985**, *15(10)*, 1438-1439.
17. Balakshy, V.I.; Voloshin, A.S.; Molchanov, V.Ya. Influence of acoustic energy walk-off on acousto-optic diffraction characteristics. *Ultrasonics* **2015**, *59(102)*, 1-7; **doi:** 10.1016/j.ultras.2015.02.002.
18. Pinnow, D.A.; Van Uitert, L.G.; Warner, A.W.; Bonner, W.A. Lead molybdate: a melt-grown crystal with a high figure of merit for acousto-optic device applications. *Appl. Phys. Lett*. **1969**, *15(3)*, 83-86; **doi:** doi.org/10.1063/1.1652917.
19. Antonov, S.N.; Mirgorodsky, V.I. Anisotropic acoustooptic modulator of nonpolarized light based on diffraction by a slow acoustic wave in a paratellurite crystal. *Techn. Physics* **2004**, *49(1)*, 83-86; **doi:** doi.org/10.1134/1.1642684.